Tropical Convective Variability as 1/f Noise

JUN-ICHI YANO, KLAUS FRAEDRICH, AND RICHARD BLENDER

Meteorologisches Institut, Universität Hamburg, Hamburg, Germany

ABSTRACT

Evidence is presented that the tropical convective variability behaves as 1/f noise for a 1–30-day period. This behavior is shown by analyzing the time series of convective available potential energy, which measures the degree of convective instability, as well as the boundary layer moisture and temperature for the 4-month period over the western Pacific during the Tropical Ocean and Global Atmosphere Coupled Ocean–Atmosphere Response Experiment. The long memory of 1/f noise associated with tropical convective variability has important implications for global climate modeling, particularly for ENSO predictions. A simple conceptual model is proposed to explain the 1/f-noise behavior.

1. Introduction

The 1/f noise, ubiquitous in nature (Hooge 1976), is defined as a time series that has a power spectrum of the form $S(\omega) \sim \omega^{-1}$, where ω is the frequency (Keshner 1982; Schuster 1988). This choice of the unit power exponent is unique in the sense that the most likely change ("variability") $\langle | \overline{x(t + \Delta t)}^{\Delta t} - \overline{x(t)}^{\Delta t} | \rangle$ of this time series over a timescale Δt does not change with increasing timescale Δt. Here, $\langle \rangle$ refers to the average of the (stationary) whole time series (or ensemble average), and the overbar $\overline{(\ )}^{\Delta t}$ is the moving average for Δt. This definition is akin to the structure function in statistical fluid dynamics (cf. Monin and Yaglom 1975), but the latter takes the square and does not apply the moving average. Such variability decreases with Δt for a "well-behaved" time series but increases with Δt for some time series such as the Brownian motion. More general, for a time series with a power spectrum $S(\omega) \sim \omega^{-\beta}$, we obtain

$$\langle | \overline{x(t + \Delta t)}^{\Delta t} - \overline{x(t)}^{\Delta t} | \rangle \sim \Delta t^{(\beta-1)/2}$$

(Yano et al. 2000; Voss 1985), and $\beta = 1$ provides a critical value. This character of 1/f noise, furthermore, leads to a long memory, and its autocorrelation only decays logarithmically with time (Hooge and Bobbert 1997).

The 1/f noise is believed to be a consequence of intermittency and stochasticity of a physical system, as shown by simple dynamical systems (Schuster 1988).

Intermittent interruptions of a "laminar" state by "turbulent" states are common features in various fluid motions. The 1/f noise also indicates contributions of infinitely many subcomponents in the system. An infinite series of resistor–capacitor circuits (Keshner 1982) is a specific example. Models for self-organized criticality provide a more general framework for such systems (cf. Bak and Chen 1991).

The current paper presents evidences that tropical convective variability behaves as 1/f noise. Considering the above physical implications of 1/f noise, this finding has a significant consequence for stochasticity of the tropical climate system, as further discussed in the last section.

2. Analyses

a. Datasets

Here, we present the results obtained by analyzing the Tropical Ocean and Global Atmosphere Coupled Ocean–Atmosphere Response Experiment (TOGA COARE) soundings during November 1992–February 1993. The TOGA COARE field experiment was performed over the western Pacific Ocean during this period (Webster and Lucas 1992). The sounding system was a part of major efforts of this experiment. The thirteen stations (see Table 1) were chosen based on data continuity and quality. TOGA COARE soundings are known suffer from moisture bias. To minimize this effect, corrected data by Lucas and Zipser (2000) are used for the three Intensive Flux Array stations (station Nos. 5, 7, and 9). The other data are as delivered by the TOGA COARE data office. The soundings were performed every 6 h, apart from the stations marked by an asterisk in the table, which were 12-hourly. Missing data

Corresponding author address: Jun-Ichi Yano, c/o Peter Bechtold, Laboratoire d'Aerologie, Observatoire Midi-Pyrenees, 14 av. Ed. Belin, 31400 Toulouse, France.
E-mail: jun-ichi.yano@aero.obs-mip.fr

Table 1. List of the TOGA COARE radiosonde stations used for this study.

Station No.	Station name	Lat	Long (°E)	Altitude (m)	Total No. of soundings
1	Thursday Island	10.6°S	142.2	61	200
2	Misima	10.7°S	152.8	7	385
3	Honiara	9.4°S	160.0	56	200
4	Santa Cruz*	10.7°S	165.8	24	168
5	Kavieng	2.6°S	150.8	3	318
6	Kapingamarangi	1.1°N	154.8	3	275
7	R/V Shiyan 3	2.4°S	157.9	4	122
8	Nauru	0.5°S	166.9	30	324
9	R/V Kexue 1	4.0°S	156.0	24	296
10	Chuuk	7.4°N	151.8	3	353
11	Pohnpei	7.0°N	158.2	39	349
12	Kwajalein*	8.7°N	167.7	4	204
13	Majuro*	7.1°N	171.4	3	209
	Total				3929

were linearly interpolated for the analyses. Note that the conclusions from the following analyses do not change by replacing it by cubic interpolation. The station numbers are given in the first column for later reference.

b. Convective variability and CAPE

We present our analysis of tropical convective variability in terms of convective available potential energy (CAPE). CAPE is widely accepted as a good measure of conditional instability of the tropical atmosphere (cf. Emanuel 1994), from which the tropical convective variability emanates. CAPE is defined as the work due to buoyancy obtained by adiabatically lifting a unit air mass from the surface boundary layer to the top of the positively buoyant layer [level of neutral buoyancy (LNB)] that is,

$$\text{CAPE} = \int_0^{\text{LNB}} B \, dz, \tag{1}$$

where buoyancy $B = (T_p - T_a)/T_a$ is defined by the virtual temperature T_p of the lifted parcel and T_a of the environmental air (as directly given by soundings). Positive buoyancy generated by heating from water condensation performs positive work on the air mass and consequently induces convective instability in the tropical atmosphere. CAPE can be defined in two ways depending on whether we assume complete removal of condensed water (pseudoadiabatic) or retain all condensed water within the lifting air mass (reversible). Here, the boundary layer values are defined as the average over the lowest 50 hPa (about 500 m) of the atmosphere. The algorithms used in this study are identical to those in G. Roff and J.-I. Yano (2001, unpublished manuscript), which will report on the other aspects of tropical convective variability inferred from this CAPE analysis.

c. Spectrum analysis

The frequency spectra of these two types of CAPE for the 13 sounding stations are presented in Fig. 1. Here, the numbers on the curves correspond to the station numbers in Table 1. Each spectrum curve is shifted by an arbitrary unit in order to show them separately. The power spectrum is defined as a square of the absolute value of the complex Fourier coefficient for a given frequency. No tapering has been applied to the time series in computing complex Fourier coefficients by the fast Fourier transform. The current time series, practically consisting of series of pulselike events (see Fig. 2a), do not require this procedure to remove the edge effects. Virtually identical results were obtained by tapering 20% of both sides of the time series in the following analysis. Note also that the "frequency" is defined by *cycle per period* as is common in engineering. In showing the individual spectra, smoothing is applied by averaging over $r_s \omega$ points centered around the frequency ω of the spectrum in concern, but solely for the graphic presentations. Here, we took $r_s = 60$ (days). Note that this smoothing has an artificial effect of broadening the diurnal-cycle peak as seen in the following examples.

In addition, a composite spectrum for all stations is shown by the thick solid curves. The composite is defined as an arithmetic mean of the normalized spectra for the individual stations. Here, the individual station spectrum is normalized to a unit total energy before the composite. No smoothing is applied to the composite spectra.

The slope for $1/f$ noise is indicated by two long-dash lines: one matched to the composite spectrum, and the other below the individual spectrum curves so that the general tendency of individual stations following this slope can be examined.

It is seen that CAPE spectra often follow this slope for periods of 1–30 days, for more than a decade. This is a wide range, considering the total frequency range of two decades in the data. Major exceptions are stations No. 2 and No. 3 for reversible CAPE. Inspection of the time series reveals that these stations do not represent much variability in reversible CAPE. The fit of the composite spectra to $1/f$ noise is much better than for the individual ones: they fit $1/f$ noise well for the whole spectrum range apart from a peak for the diurnal cycle. For reference, the 95% confidence interval assuming the χ^2 distribution of the errors (cf. Jenkins and Watts 1968) is marked by the short-dash lines relative to the $1/f$-noise slope attached to the composite spectrum. Here, 26 degrees of freedom are assumed, consistent with the total number of stations (multiplied by 2, taking into account the number of degrees of freedom of an individual spectrum). It shows that no fluctuation of this composite besides the diurnal-cycle peak deviates from the $1/f$-noise spectrum with 95% confidence for both pseudoadiabatic and reversible CAPE.
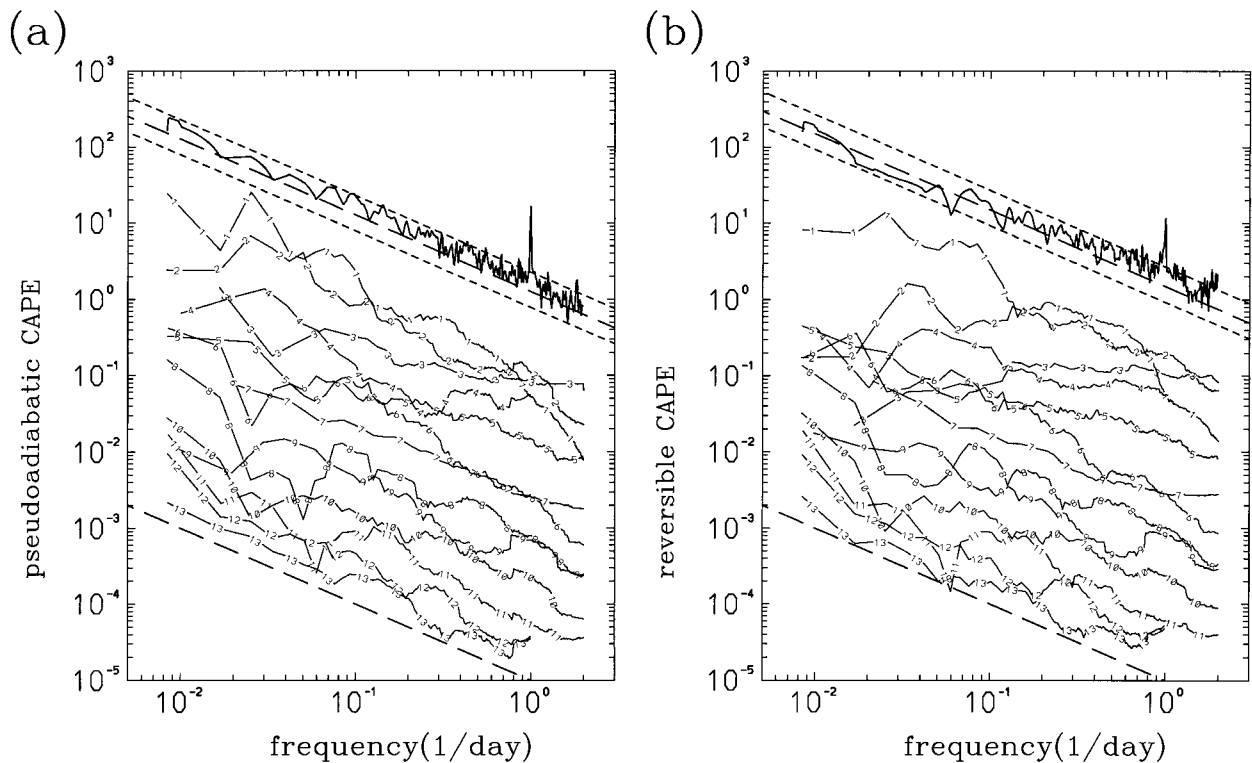
FIG. 1. The frequency spectra of (a) pseudoadiabatic and (b) reversible CAPE for the 13 TOGA COARE stations. Numbers on curves correspond to the station numbers in the first column of Table 1. Each spectrum curve is shifted by an arbitrary unit in order to show them separately. In addition, the composite spectrum for all 13 stations is shown by a thick solid curve. The slope for $1/f$ noise is indicated by two long-dash lines: one matched to the composite spectrum, and the other to the bottom of frame so that a general tendency of individual station to follow this slope can be examined. The 95% confidence interval assuming the χ^2 distribution is also shown by two short-dash lines relative to the long-dash line attached to the composite.

d. Detrended fluctuation analysis

Another way of providing a quantitative estimate of the spectrum slope and the validity range is the detrended fluctuation analysis (DFA; Peng et al. 1994; Koscielny-Bunde et al. 1998). DFA determines the long-time behavior of the correlations and the power spectrum by a scale-selective fluctuation analysis of the time series.

For this analysis, the original time series is normalized by its variance after subtracting the mean, to obtain the standardized time series, say, x_i ($i = 1, \ldots, N$), where N is the total number of measurements. Then, x_i is integrated to obtain a random walk, or a profile, $y_j = \sum_{i=1}^{j} x_i$. An example of standardized CAPE time series and the resulting profile are shown in Figs. 2a and 2b, respectively.

The fluctuations (variances) of the profile are calculated for the all segments of the time series after subtracting a linear trend. In each segment range ($j, j + s - 1$) of length s, the fluctuations are defined by $F_j(s) = [1/s \sum_{i=j}^{j+s-1} (y_i - \tilde{y}_i)^2]^{1/2}$, where $\tilde{y}_i$ is the linear trend in the particular segment. The final result for the fluctuations is given by averaging over either all possible overlapping ($N - s + 1$) or nonoverlapping (N/s) seg-

ments. The obtained fluctuations $F(s)$ from the profile in Fig. 2b are shown in Fig. 3 for the overlapping and the nonoverlapping cases by the triangles and the circles, respectively.

It is seen that $F(s)$ with the overlapping segments is smoother than the nonoverlapping case, because of a higher number of samples available with the former choice, which further reduces the statistical errors of the analysis. For this reason, the fluctuations $F(s)$ using the overlapping segments are used in the following analyses.

If the power spectrum follows a power law, $S(\omega) \sim \omega^{-\beta}$, the fluctuation follows $F(s) \sim s^\alpha$, whose exponent α defines the power exponent by $\beta = 2\alpha - 1$. Furthermore, we define the frequency range of validity by the longest segment in which $F(s)$ deviates less than a threshold ϵ from the optimized fitting s^α on the log–log plot (with the base of 10). Here, $\epsilon = 0.02$ in this analysis. The optimized slope and range are indicated by a solid line segment in Fig. 3. The threshold ϵ is also marked. The exponents β and the validity ranges of the power law for the CAPE spectra are estimated by DFA in this way and are listed in Table 2. The ensemble-averaged values are shown in the bottom row.
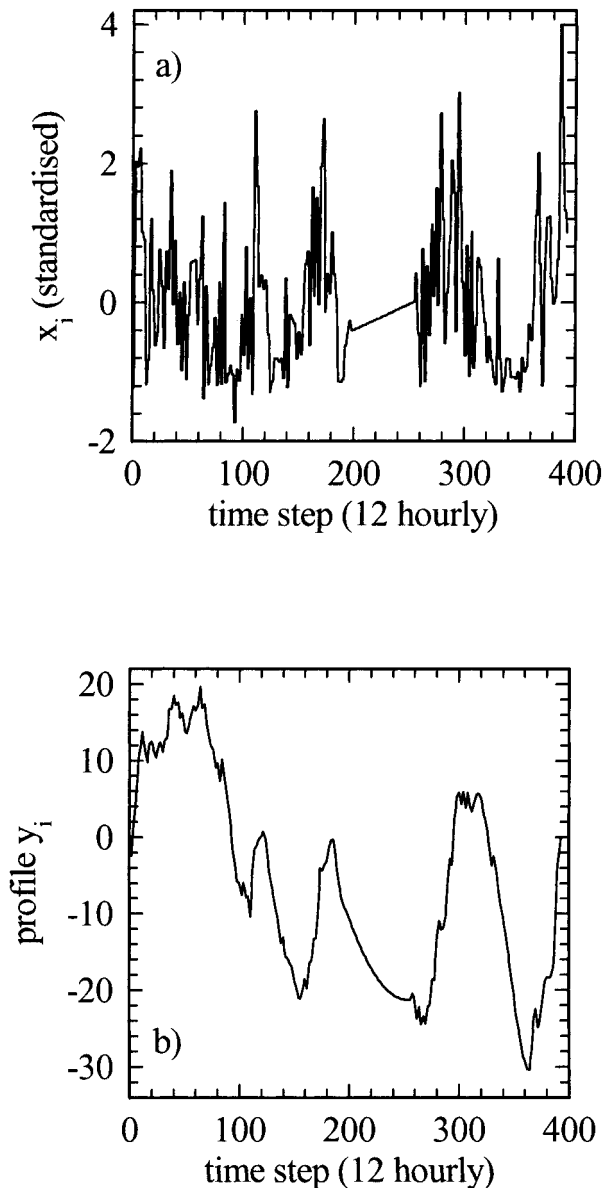
FIG. 2. An example of (a) standardized CAPE time series and (b) the resulting profile. A station taken is Santa Cruz (No. 4).
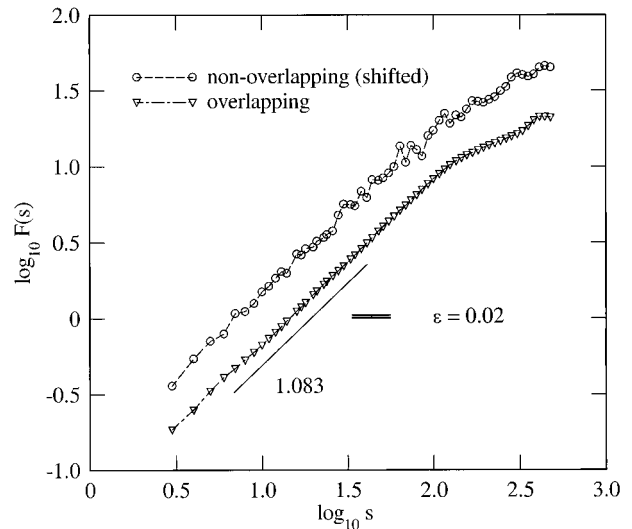

FIG. 3. The fluctuation $F(s)$ as a function of the segment length (nondimensional timescale) s obtained from the profile in Fig. 2b. The triangles and the circles (shifted) show the results for the overlapping and nonoverlapping segments, respectively. The optimized fit to the power law ($\beta = 1.083$) to the overlapping case is shown by attaching a straight line to the validity range with the threshold $\epsilon = 0.02$, also shown by a vertical bar to the right.

The ensemble average of the exponent of pseudoadiabatic-CAPE spectra is almost perfectly $1/f$ noise, although the exponents for individual stations vary substantially. On the other hand, in ensemble mean, the reversible-CAPE spectrum shows a slightly gentler slope than $1/f$ noise. Note that, practically, a power exponent in the range 0.8–1.4 is considered as $1/f$ noise (Keshner 1982; Schuster 1988).

Here, the ensemble-averaged exponent is defined as an average weighted by the validity range in logarithmic scale. The mean validity range, defined by the geometric means (i.e., arithmetic means in the logarithmic scale) of the minimum and the maximum periods, is approx-

imately one decade for both types of CAPE, and some stations represent a much wider validity range. It is emphasized that the estimate of the validity ranges is conservative because of the choice of the small threshold ϵ, and extension of the range is often feasible by visually inspecting the fluctuation $F(s)$ (cf. Fig. 3). This is alternatively achieved by slightly increasing ϵ. On the other hand, it was found that the estimated exponent β is generally stable against the change of threshold.

e. Analysis of the other variables

What is responsible for $1/f$-noise behavior of CAPE? It is known that tropical convective instability is strongly controlled by the atmospheric boundary layer moisture and temperature (e.g., Kingsmill and Houze 1999). Hence, it is likely that CAPE variability is also under a strong control by the boundary layer variables. To examine this, we separate CAPE into the boundary layer (with subscript b) and the tropospheric (subscript t) components as follows:

$$CAPE = CAPE_b + CAPE_t,$$

where

$$CAPE_b = \int_0^{LNB} (T_p - \overline{T}_a)/T_a \, dz,$$

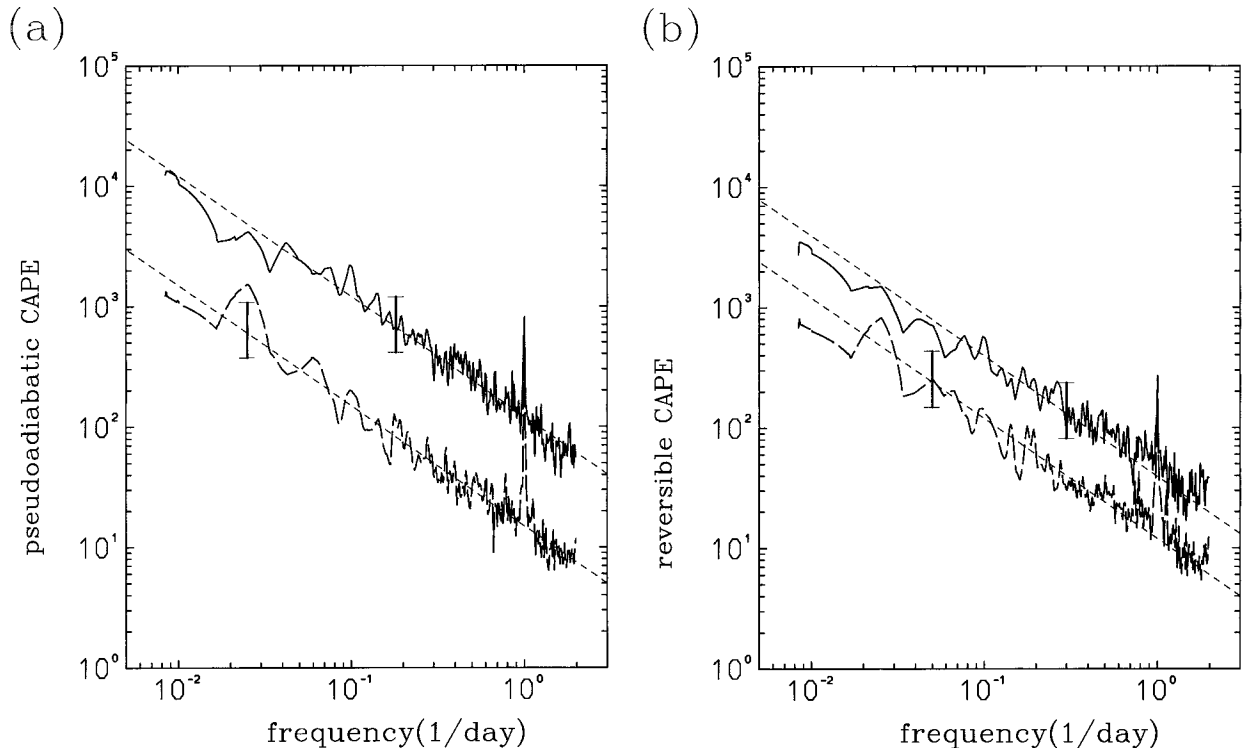$$CAPE_t = \int_0^{LNB} (\overline{T}_a - T_a)/T_a \, dz,$$

FIG. 4. Composite spectra for the (a) pseudoadiabatic and (b) reversible CAPE separated into the boundary layer (solid) and tropospheric components (long dash). The 95% confidence intervals are shown by bars relative to the optimized fit (short dash) curves.

and $\overline{T}_a$ is the mean environmental virtual temperature profile for each station. Note that $\overline{T}_a$ only serves as a reference to define the fluctuating parts of T_p and T_a, and the overall structure of spectra should not depend on the exact definition of the reference.

Composite spectra for these decomposed CAPE components are shown in Figs. 4a and 4b for the pseudoadiabatic and reversible cases, respectively. Here, spectra for $CAPE_b$ and $CAPE_t$ are depicted by the solid and the long-dash curves, with the 95% significance interval indicated by a bar relative to straight lines (short dash) corresponding to $1/f$ noise. The composite is defined as an arithmetic mean of the normalized station spectra. The absolute value of the spectra is recovered by multiplying the geometrical mean of the total spectrum energy for the individual stations. This somewhat-involved composite procedure was found to be necessary, because the frequency range is different for each spectrum.

Both figures show that most of CAPE variability is due to the boundary layer variability. The tropospheric contribution is only 10% for the pseudoadiabatic CAPE and 30% for the reversible CAPE. It is also seen that the boundary layer component of CAPE represents a $1/f$-noise spectrum within 95% confidence. The ensemble-averaged exponents estimated from DFA are $\beta = 0.94$ and 0.78 for the pseudoadiabatic and reversible

cases, respectively, with an approximate period of validity given by 2–20 days. On the other hand, the tropospheric component represents a statistically significant deviation from $1/f$ noise in the intraseasonal scale (30–50 days).

To see the role of boundary layer variability more directly, the frequency spectra of the boundary layer moisture and temperature are presented in Figs. 5a and 5b, respectively. Both spectra are plotted in the same format as in Fig. 1. These two variables follow $1/f$-noise behavior equally well as CAPE in a wide frequency range. The objectively defined exponents and the validity ranges by DFA are also listed in Table 2. The boundary layer moisture almost perfectly follows $1/f$ noise for the 1–10-day period, whereas the boundary layer temperature represents a gentler exponent slope but still sufficiently close to $1/f$ noise in ensemble average. The validity range is wider in the latter case.

On the other hand, the vertically averaged tropospheric moisture and temperature (averaged over 0–16 km) shown in Figs. 6a and 6b, respectively, follow a steeper exponent. The moisture spectrum slope is $\beta \simeq 5/3$ for higher frequencies above 10^{-1} days^{-1} as shown by a long-dash line for fit and a confidence interval indicated by two short-dash lines. Although the composite temperature spectrum is not as steep as that of moisture, the slope still deviates significantly from that
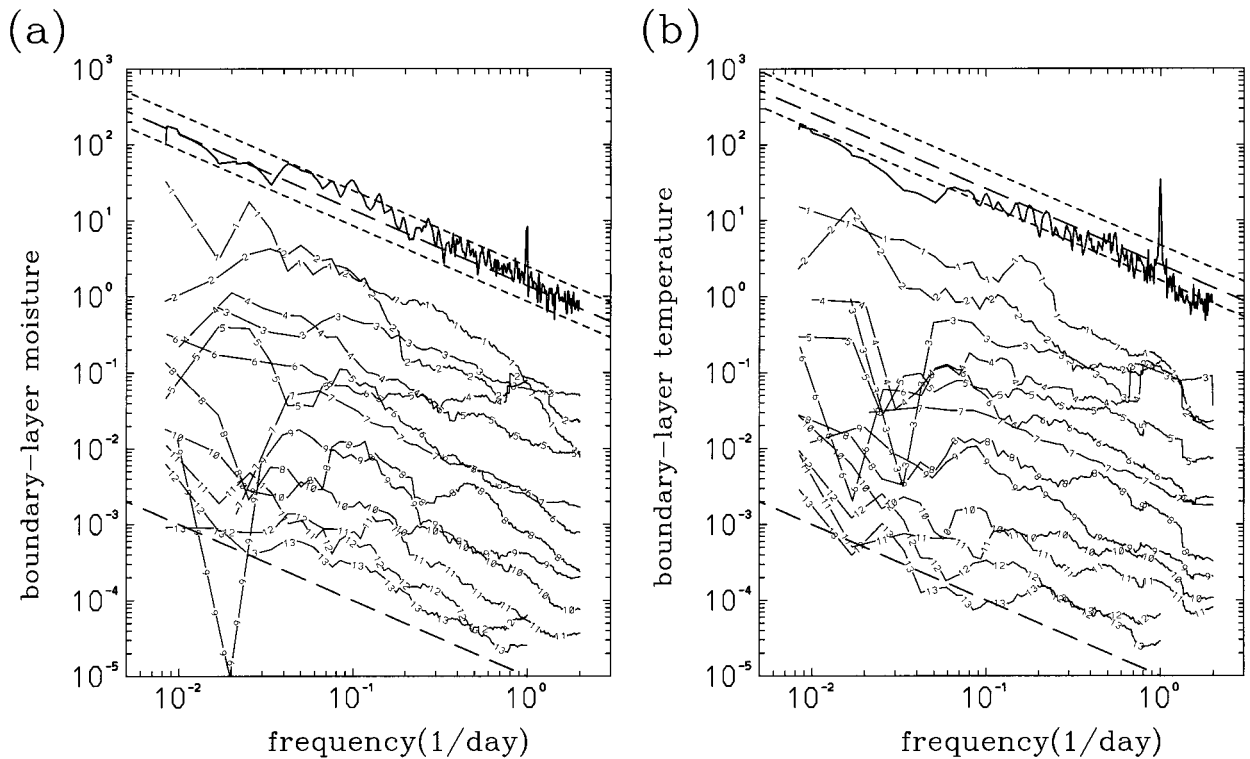
FIG. 5. The same as in Fig. 1 but for boundary layer (a) moisture and (b) temperature.

of $1/f$ noise. The slope for some individual spectra can be much steeper. Hence, we conclude that $1/f$ noise CAPE behavior is a consequence of a similar variability in the boundary layer moisture and temperature. Furthermore, we found that the LNB, which measures the potential height of cumulus convective towers, also varies as $1/f$ noise (not shown).

3. Discussion

a. Physical interpretation

The physical mechanism for $1/f$ noise in tropical convection is yet to be developed. Nevertheless, the recent theoretical model for $1/f$ noise by Kaulakys and Meskauskas (1998) provides some hints on this issue. They showed that a particular construction of a random series of pulselike events produces $1/f$ noise. In this construction, the intervals between the pulselike events are predicted by a first-order autoregression model with Gaussian white-noise forcing and a relaxation to a mean interval τ by a constant rate γ. According to this theory, the system behaves as $1/f$ noise for the timescales from τ to τ/γ, when the fluctuation of the time interval is of the same order of magnitude as the mean interval τ and when the relaxation rate γ is small enough.[1]

A simple physical picture for $1/f$ noise can also be obtained in this limit. The pulselike events tend to recur quasi-periodically with an approximate period τ, providing a long memory. However, this is constantly randomized by white-noise perturbation against a weak restoration force.

In the tropical convective atmosphere, each cumulus convective event can be considered as such a pulselike event in the above theory. In the atmospheric boundary layer, this is characterized by a sudden decrease of moisture and temperature, due to convective downdrafts, which is immediately followed by a sudden recovery of these values (e.g., Jorgensen et al. 1997; Saxen and Rutledge 1998; Halverson et al. 1999). This also produces a corresponding pulselike behavior of CAPE. The interval of one convective event to the next may be estimated as a few hours to a few days, with a mean value $\tau \simeq 1$ day. With $\gamma \simeq 3 \times 10^{-2}$, we obtain $1/f$ noise for the timescales of 1–30 days. Here, it is interesting to note that the low-frequency end of $1/f$ noise corresponds to the intraseasonal scale, on which the variability is dominant in the tropical atmosphere as manifested as the Madden–Julian oscillation (Madden and Julian 1994).

b. Implications for climate dynamics

This picture for tropical convective variability may urge a drastic change of its treatment in global climate

---

[1] We also neglect the factor 2π in the above argument for simplicity, which is formally justified when τ is redefined as $2\pi\tau$.
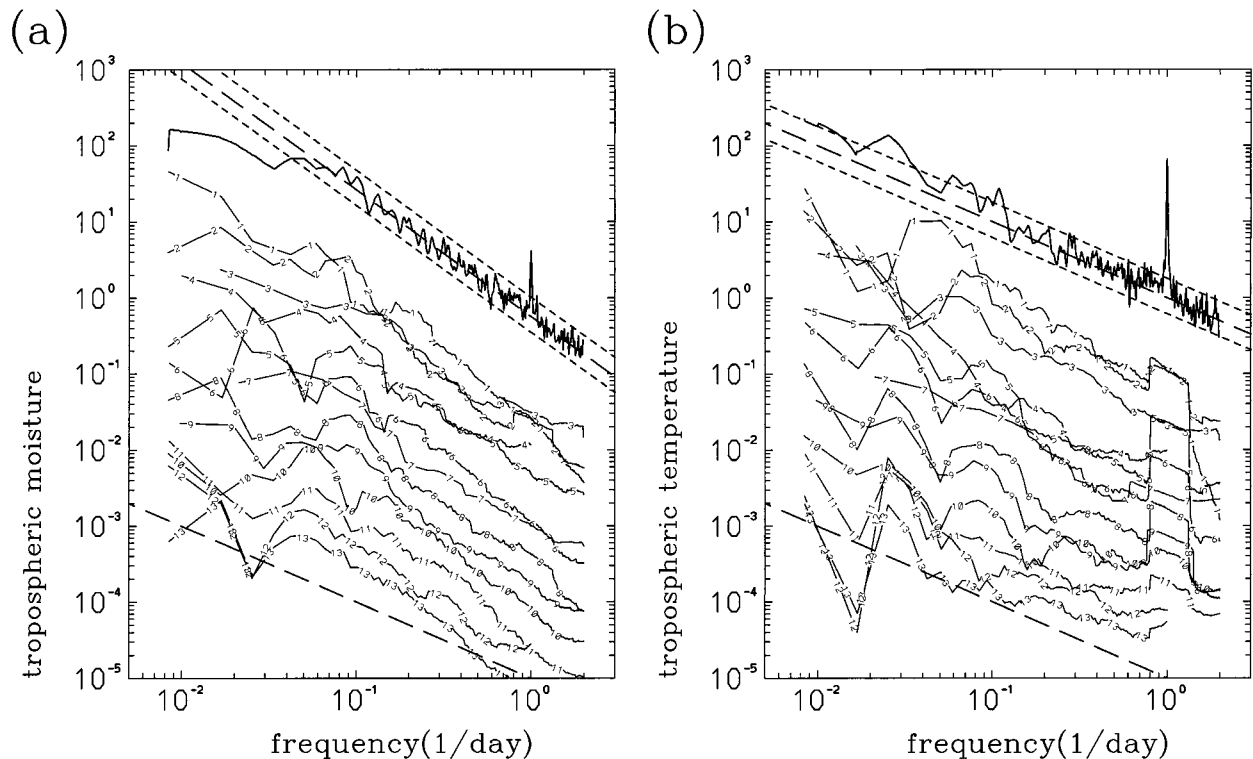
FIG. 6. The same as in Fig. 1 but for tropospheric-averaged (0–16 km) (a) moisture and (b) temperature. The slope for fit to the composite is changed to $\beta = 5/3$ in (a).

models. It has been treated traditionally in terms of ensemble average, assuming instantaneous equilibrium with the large-scale dynamics (cf. Arakawa and Schubert 1974). On the other hand, our new picture suggests that the individual pulselike convective events play more intrinsic roles in the dynamics. Such a process may not be described in a simple ensemble-averaged sense by scale separation. Instead, this suggests that the tropical convective system deviates inherently from equilibrium by shifting back and forth between the destabilized convective periods and "overstabilized" (in the sense that convection is unlikely to be triggered easily) nonconvective periods. Hence, a radically different cumulus parameterization is required, based on the $1/f$-noise picture of tropical convection.

A long memory of convective pulse events may also have a profound impact on the long-term predictability of the atmosphere. In current ENSO modeling (e.g., Penland and Sardeshmukh 1995; Kleeman and Moore 1997; Kestin et al. 1998; Moore and Kleeman 1999), the tropical convective variability is considered only as white-noise forcing that has no memory by itself. The current finding suggests that a fundamentally different type of stochastic forcing may be required for these modelings. It is interesting to note that intraseasonal variability (Madden–Julian oscillation) has been speculated to be an important trigger for El Niño events (cf. Moore and Kleeman 1999). This speculation may be

better associated with the long memory of convective variability for a wider frequency range.

The $1/f$-noise description of convective variability may, furthermore, improve the modeling of the stratospheric quasi-biennial oscillation (QBO). Ricciardulli and Garcia (2000) showed that the National Center for Atmospheric Research Community Climate Model convective parameterizations do not produce sufficient high-frequency forcing necessary to generate QBO. A lack of high-frequency variability is, ironically, consistent with and a logical consequence of the scale-separation principle on which their parameterization is based. The $1/f$ noise can more directly provide these high-frequency variabilities necessary for QBO.

c. Limitations of this analysis

A highly spiky nature of $1/f$ noise expected from Kaulakys and Meskauskas's (1998) model is evident from direct inspections of time series of the convective variables (cf. Fig. 2a). Nevertheless, the individual convective events are not resolved in the sounding dataset with 6–12-h intervals. Direct examinations of these individual convective events are still awaited by using more frequent soundings or equivalent remote sensing measurements.

Another limitation of this analysis is in its restriction to the single-point measurements by the soundings. As-

TABLE 2. The power exponent and the validity range (given in the parentheses: the periods in days) determined by DFA for the variables listed in the header. The corresponding station names are given in the first column. The mean values are shown in the bottom row. The mean exponent is defined by weighting the validity range logarithmically. The mean minimum and maximum periods are computed by geometric means. Note that the last digits of the values in the table are the order of the analysis errors.

Station name	Pseudoadiabatic CAPE Exponent (range)	Reversible CAPE Exponent (range)	Boundary layer moisture Exponent (range)	Boundary layer temperature Exponent (range)
Thursday Island	1.36 (1.7–45)	1.27 (2.5–15)	1.16 (3.1–45)	0.86 (3.9–31)
Misima	1.17 (1.7–10)	0.69 (1.6–7.1)	1.27 (1.0–3.9)	1.08 (1.9–36)
Honiara	0.78 (3.4–31)	0.04 (1.9–10)	0.25 (3.6–19)	0.37 (1.2–8.2)
Santa Cruz*	1.08 (5.0–35)	0.37 (3.0–58)	0.73 (2.2–7.2)	0.50 (2.8–14)
Kavieng	0.56 (1.7–22)	0.47 (1.5–25)	0.57 (1.9–15)	0.44 (2.5–27)
Kapingamarangi	1.42 (1.3–6.6)	0.36 (4.2–53)	1.40 (1.1–10)	0.90 (1.7–12)
R/V Shiyan 3	0.88 (0.9–23)	0.82 (1.4–20)	0.87 (1.3–14)	0.86 (1.4–11)
Nauru	0.88 (1.6–11)	0.74 (1.4–13)	0.84 (1.7–10)	0.68 (1.9–13)
R/V Kexue 1	0.88 (1.5–34)	0.90 (2.0–19)	1.11 (1.0–7.6)	1.24 (0.7–12)
Chuuk	0.71 (2.5–27)	0.62 (2.5–15)	0.64 (3.9–42)	0.47 (1.7–25)
Pohnpei	1.18 (1.1–7.6)	1.12 (1.0–7.6)	1.28 (1.0–7.1)	0.57 (1.5–8.8)
Kwajalein*	0.99 (2.6–50)	0.83 (5.0–22)	1.14 (2.8–16)	0.68 (2.8–12)
Majuro*	0.88 (4.3–46)	0.89 (1.4–91)	1.11 (2.6–15)	0.34 (4.0–18)
Mean	0.97 (2.0–22)	0.70 (2.0–20)	0.96 (1.9–13)	0.72 (1.9–16)

pects of the spatial-scale dependence of $1/f$ noise are still to be investigated fully. Nevertheless, $1/f$-noise behavior is likely to be robust against the spatial averaging. Simple mathematical considerations show that a power-spectrum shape (but not the amplitude) should be strictly preserved in the two opposite limits: both when the variability is spatially totally uncorrelated and when it is in perfect coherency. Indeed, reexamination of earlier work (Yano and Nishi 1989) indicates that $1/f$ noise can still be identified in the outgoing longwave radiation averaged over a $2.5° \times 2.5°$ grid box, and the observed spatial coherency of tropical convective variability suggests that this conclusion can be extrapolated further to a larger scale.

REFERENCES

Arakawa, A., and W. H. Schubert, 1974: Interaction of a cumulus cloud ensemble with the large-scale environment, Part I. *J. Atmos. Sci.,* **31,** 674–701.

Bak, P., and K. Chen, 1991: Self-organized criticality. *Sci. Amer.,* **264** (January), 26–33.

Emanuel, K. A., 1994: *Atmospheric Convection.* Oxford University Press, 580 pp.

Halverson, J. B., B. S. Ferrier, T. M. Rickenbach, J. Simpson, and W. K. Tao, 1999: An ensemble of convective systems on 11 February 1993 during TOGA COARE: Morphology, rainfall characteristics, and anvil cloud interactions. *Mon. Wea. Rev.,* **127,** 1208–1228.

Hooge, F. N., 1976: $1/f$ noise. *Physica B,C,* **83,** 14–23.

——, and P. A. Bobbert, 1997: On the correlation function of $1/f$ noise. *Physica B,* **239,** 223–230.

Jenkins, G. M., and D. G. Watts, 1968: *Spectrum Analysis and Its Application.* Holden-Day, 525 pp.

Jorgensen, D. P., M. A. LeMone, and S. B. Trier, 1997: Structure and evolution of the 22 February 1993 TOGA COARE squall line: Aircraft observations of precipitation, circulation, and surface energy fluxes. *J. Atmos. Sci.,* **54,** 1961–1985.

Kaulakys, B., and T. Meskauskas, 1998: Modeling $1/f$ noise. *Phys. Rev. E,* **58,** 7013–7019.

Keshner, M. S., 1982: $1/f$ noise. *Proc. IEEE,* **70,** 212–218.

Kestin, T. S., D. J. Karoly, J. I. Yano, and N. A. Rayner, 1998: Time-frequency variability of ENSO and stochastic simulations. *J. Climate,* **11,** 2258–2272.

Kingsmill, D. E., and R. A. Houze, 1999: Thermodynamic characteristics of air flowing into and out of precipitating convection over the West Pacific warm pool. *Quart. J. Roy. Meteor. Soc.,* **125,** 1209–1229.

Kleeman, R., and A. M. Moore, 1997: A theory for the limitation of ENSO predictability due to stochastic atmospheric transients. *J. Atmos. Sci.,* **54,** 753–767.

Koscielny-Bunde, E., A. Bunde, S. Havlin, H. E. Roman, Y. Goldreich, and H.-J. Schellnhuber, 1998: Indication of a universal persistence law governing atmospheric variability. *Phys. Rev. Lett.,* **81,** 729–732.

Lucas, C., and E. J. Zipser, 2000: Environmental variability during TOGA COARE. *J. Atmos. Sci.,* **57,** 2333–2350.

Madden, R. A., and P. R. Julian, 1994: Observations of the 40–50-day tropical oscillations—a review. *Mon. Wea. Rev.,* **122,** 814–837.

Monin, A. S., and A. M. Yaglom, 1975: *Statistical Fluid Mechanics: Mechanics of Turbulence.* Vol. 2. MIT Press, 874 pp.

Moore, A. M., and R. Kleeman, 1999: Stochastic forcing of ENSO by the intraseasonal oscillation. *J. Climate,* **12,** 1199–1220.

Peng, C.-K., B. V. Buldyrev, S. Havlin, M. Simons, H. E. Stanley, and A. L. Goldberger, 1994: Mosaic organization of DNA nucleotides. *Phys. Rev. E,* **49,** 1685–1689.

Penland, C., and P. D. Sardeshmukh, 1995: The optimal growth of tropical sea surface temperature anomalies. *J. Climate,* **8,** 1999–2024.

Ricciardulli, L., and R. R. Garcia, 2000: The excitation of equatorial waves by deep convection in the NCAR Community Climate Model (CCM3). *J. Atmos. Sci.,* **57,** 3461–3487.

Saxen, T. R., and S. A. Rutledge, 1998: Surface fluxes and boundary layer recovery in TOGA COARE: Sensitivity to convective organization. *J. Atmos. Sci.,* **55,** 2763–2781.

Schuster, H. G., 1988: *Deterministic Chaos.* 2d ed. VCH Verlagsgesellschaft, 270 pp.

Voss, R. F., 1985: Random fractal forgeries. *Fundamental Algorithms in Computer Graphics,* R. A. Earnshaw, Ed., Springer Verlag, 805–835.

Webster, P., and R. Lukas, 1992: TOGA COARE: the Coupled Ocean–Atmosphere Response Experiment. *Bull. Amer. Meteor. Soc.,* **73,** 1377–1416.

Yano, J. I., and N. Nishi, 1989: The hierarchy and self-affinity of the time variability within the tropical atmosphere inferred from the NOAA OLR data. *J. Meteor. Soc. Japan,* **67,** 771–789.

——, W. W. Grabowski, G. L. Roff, and B. E. Mapes, 2000: Asymptotic approaches to convective quasi-equilibrium. *Quart. J. Roy. Meteor. Soc.,* **126,** 1861–1887.